JOURNAL OF MATERIALS SCIENCE 28 (1993) 3103–3115

The influence of Saffil δ-alumina fibre reinforcement on gas entrapment and evolution in P/M Al–20Si–3Cu–1Mg–x Al_2O_3 composite

J. H. TER HAAR, J. DUSZCZYK
Laboratory of Materials Science, Delft University of Technology Rotterdamseweg 137, 2628 AL, Delft, The Netherlands

Compacts of an aluminium/alumina fibre composite, produced by a powder metallurgical (P/M) route, were the subject of a vacuum degassing study. The materials consisted of Al–20 wt % Si–3 wt % Cu–1 wt % Mg pre-alloyed powder mixed with 0%, 5% and 20% (by volume) of Saffil δ-alumina fibres. The composition of gases liberated during heating at constant rate was monitored with a quadrupole mass spectrometer. Water and hydrogen were the main volatile products released. High water and hydrogen pressures were maintained longest by the composite with the highest volume fraction of fibres. The presence of fibres gave rise to delayed peak hydrogen production when compared to the matrix. Nitrogen adsorption analysis proved that the Saffil fibre RF Milled, possesses a large specific internal surface area and points towards the presence of very fine-sized porosity. Thermogravimetric analyses confirmed a high water content of the fibres of at least 0.86 wt %. Of this, condensed and adsorbed water constitute the largest fraction. Owing to the fineness of the porosity and consequently the low concentration gradients, time as well as temperature (for enhancement of diffusion) are equally important variables to be considered for effective degassing of these composites.

1. Introduction

By reinforcing P/M aluminium alloys with short alumina fibres one may aim at a better retention of elevated temperature strength and increases in modulus and wear resistance. These intended improvements will, among others, depend on the quality and stability of the interfacial bond. It seems reasonable to assume that volatile phases entrapped during consolidation may affect the quality of the interface, and by that, deteriorate mechanical properties.

Atomized aluminium powders normally require some form of a degassing treatment prior to consolidation. This is to lower the surface moisture content which can be considerable owing to the high specific surface area of powders in general. The detrimental effect of surface moisture is present in a latent sense when it becomes entrapped in the (partially dense) solid. During subsequent elevated temperature processing, or while at high-temperature service conditions, conversion to hydrogen may occur. Material defects then may arise due to the mobility of the hydrogen under these conditions.

For P/M aluminium composites, the degassing step of the processing does require special attention because the ceramics involved (oxides, nitrides, carbides, borides) do not unusually possess hydrophylic surfaces [1]. Moreover, processing routes for this class of materials involve more intensive handling and air exposure than is the case for the metal powder only. Surface moisture may be important in determining the final performance of the reinforcement, with respect to the quality and stability of bonding to the metallic matrix.

The present study was conducted with the aim to compare the vacuum degassing behaviour of a pre-alloyed aluminium powder with that of a composite prepared by dry mixing of the same powder with alumina polycrystalline fibres.

2. Materials

The metal matrix composite (MMC) powders used in this study were prepared by co-milling in a ball mill air-atomized Al–20Si–3 Cu–1 Mg powder (Showa Denko K. K., Japan) and δ-alumina fibres (Saffil Milled RF grade 590, ICI, Runcorn, UK). A description of this process is given elsewhere [2]. Some data on the materials are given in Table I. The density of the ASCM20 powder was calculated by assuming a zero volume change effect of alloying. Results of chemical analyses of the aluminium powder alloy are presented in Table II. The values of the present analyses do correspond reasonably well with the producers' data except for the analysis of magnesium by inductively coupled plasma–atomic emission spectroscopy (ICP–AES). The low value may reveal an enrichment of magnesium in the powders' oxide layer, which is not dissolved and thus not analysed. X-ray fluorescence takes account of this oxide layer and shows a correct magnesium level.

0022–2461 © *1993 Chapman & Hall*

Saffil alumina fibre is produced by a low-temperature solution spinning [3] followed by a product-specific heat treatment depending on the application. During the heat treatment, the water and the organic binder are driven off and the fibre precursor is transformed into the desired crystallographic alumina modification. During heating (above 1000 °C), the fibre undergoes a number of progressive structural and crystallographic changes (Fig. 1). As the crystallinity increases with holding time, the pore volume decreases while the material experiences a sequence of transformations from phases ε to α [3]. The fibre which was presently used is the δ-alumina form of 79% crystallinity. It is stabilized by the addition of 4 wt % silica [3].

It was previously found [2] that this type of Saffil fibre possesses a large specific surface area (Table I). Because the value is approximately 40 times that which would be expected on the basis of fibre size and shape, it can only be explained by porosity and the resulting internal surface. The scanning electron micrograph of Fig. 2 provides us with some microstructural support, as porosity may be interpreted

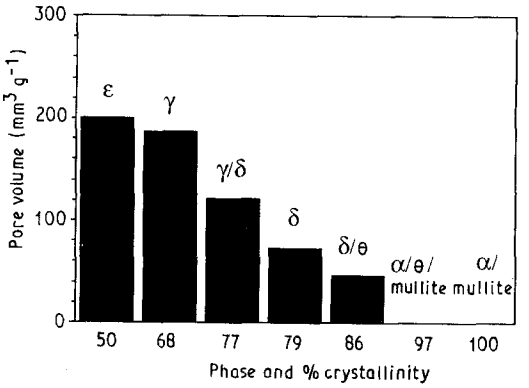

Figure 1 Progressive (sintering) sequence of crystallographic modifications, porosities and crystallinities for Saffil fibre [3].

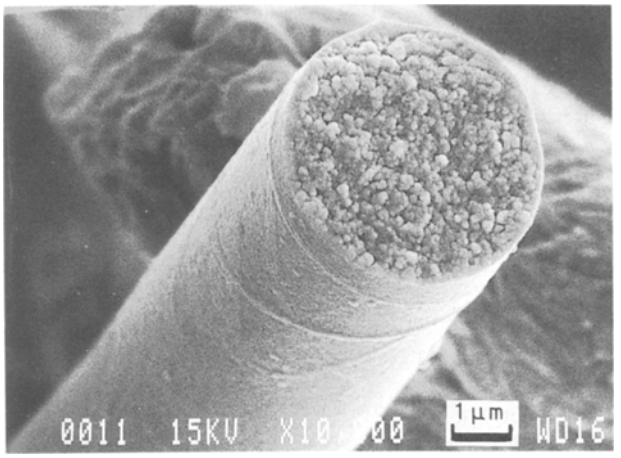

Figure 2 Scanning electron micrograph of Saffil Milled fibre showing granular structure at fracture surface.

from the granular microstructure at fracture surfaces. Pores of a visible size, however, cannot account for the high value of the specific surface area.

The large surface area implies a high potential for storage of surface moisture. Therefore, the study of outgassing of the present reinforcement may be as important as that of the matrix.

TABLE I Relevant data for the materials in this study

	ASCM20	Saffil RF Milled
Composition (wt %)	20 Si 3 Cu 1 Mg bal. Al	96–97 Al_2O_3 3–4 SiO_2
Mean size of particle/fibre	26 µm (−100 mesh)	Diameter: 3 µm Length: ~ 200 µm
Density (10^3 kg m^{-3})	2.66[a]	3.3–3.5[b] $\rho_{true,exp.}$ 3.52[c] $\rho_{theor.}$ 3.69[d] ρ_f 2.8[e]
Specific surface area (10^3m^{2}kg^{-1}) (BET method)	0.19	16.8
Pore volume: (10^{-3} m^{3}kg^{-1}/%)	–	0.073[b]/20 (excl. micropores) 0.045/14[f]

[a] Calculated with densities of constituting elements.
[b] Datasheet Saffil Fibre/ICI. [3]
[c] Determined by helium pycnometry with prior outgassing at 150 °C.
[d] Calculated from crystallographic data [4] (see Appendix A.2).
[e] Calculated using Equation 13, see text.
[f] Nitrogen adsorption/desorption analysis; micropore fraction (d < 2 nm) excluded.

3. Oxides and hydroxides of aluminium

3.1. Formation of an oxide layer on aluminium

In an ambient environment, elemental aluminium is thermodynamically unstable with respect to its oxides and hydroxides

$$2Al + 1.5O_2 \rightarrow Al_2O_3 \quad \Delta G_0 = -1583\ kJ\,mol^{-1} \quad (1)$$

TABLE II Chemical analysis (ICP–AES, unless stated otherwise) of the as-received ASCM20 powder

	Si (wt %)	Cu (wt %)	Mg (wt %)	Fe (wt %)	Mn (wt %)	Zn (wt %)
Producer	20.4[a]	3.14	1.28	0.26	0.1 max.	0.1 max.
	20.05[b]	3.14	0.60 ± 0.23	0.23	n.a.[c]	n.a.
As received	19.00[d]	3.264[d]	1.246[d]	0.289[d]	0.007[d]	0.022[d]

[a] Volumetric wet chemical analysis.
[b] Flame AAS.
[c] n.a. not analysed.
[d] XRF analysis.

where ΔG_0 is the standard Gibb's energy change of the reaction. Aluminium also readily reduces water, because the standard potential of the electrode reaction

$$1/3Al^{3+} + e^- = 1/3Al \quad (2)$$

is highly negative. During exposure of metallic aluminium to air and moisture, a surface film is formed by one or more of the following reactions (including Reaction 1)

$$2Al + 3H_2O \rightarrow Al_2O_3 + 3H_2 \quad (3)$$

$$Al + 2H_2O \rightarrow AlOOH + 1.5H_2 \quad (4)$$

$$Al + 3H_2O \rightarrow Al(OH)_3 + 1.5H_2 \quad (5)$$

After the formation of a first protective film, further reactions (with H_2O) can take place at rates which are functions of water pressure, $p(H_2O)$, and temperature, T

$$Al_2O_3 + H_2O \rightarrow 2AlOOH \quad (6)$$

$$Al_2O_3 + 3H_2O \rightarrow 2Al(OH)_3 \quad (7)$$

$$AlOOH + H_2O \rightarrow Al(OH)_3 \quad (8)$$

During exposure of metallic aluminium to dry air at room temperature an amorphous, surface oxide layer is formed of 2–4 nm thickness with an estimated density of $\sim 3.0 \times 10^3$ kg m^{-3}, providing a restrictive diffusion barrier against further oxidation [4].

Aluminium powders are usually made by melt atomization. The structure of the oxide film and the extent of its hydration depend on the atomization atmosphere and the subsequent heat treatment of the powder. There is evidence [4] that at temperatures $T > 375\,^\circ$C rates and mechanisms of aluminium oxidation are similar for dry and moist atmospheres. This would suggest that during air atomization of aluminium powders the oxide film is formed according to Reactions 1 and 3. Because of the rapid cooling, there is little time for secondary formation of hydroxides from oxides through Reactions 6–8 at elevated temperatures. However, water may be easily adsorbed at low temperatures (e.g. during storage). During cooling in the atomization atmosphere, water may also be stored within fine pores in the oxide film due to capillary condensation. Reactions 6–8 may then take place during powder storage and handling.

Roikh *et al.* [5] found that at room temperature, aluminium powders are highly stable with respect to oxidation by moisture below humidities of 80%. When temperature or humidities, however, rise above 30 °C or 80%, respectively, large increases in rate of water uptake can occur due to the reaction of oxide to form hydroxide and a corresponding rise in adsorptive capacity.

Nylund and Olefjord [6] have found that their helium-atomized Al–5Mn–6Cr powder after minimum exposure to air did release water during degassing. This implies that entrapment of moisture takes place relatively quickly at ambient temperature.

3.2. Chemical nature of the surface of crystalline alumina

Alumina exists, in addition to crystalline α-alumina, in several more crystallographic modifications grouped under the name *transition* aluminas. They cannot be considered true polymorphs of Al_2O_3, but represent various states of structural reordering. The χ-, η- and γ-modifications of alumina may form during thermal decomposition of aluminium hydroxides at low temperatures ($T < 800\,^\circ$C) and are therefore called low-temperature aluminas. The κ-, δ- and θ-aluminas may form during extended heating above 800 °C and are called high-temperature transition aluminas. Above 1100 °C, only crystalline α-alumina exists.

The surface chemistry of crystalline alumina is quite different from that of the bulk. The surface is characterized by its affinity to water. A simplified model for water at the surface of γ-alumina [7] is presented in Fig. 3. In general terms, a similar pattern may be valid for the surface of δ-alumina. In the scheme of Fig. 3, layer A represents the physically adsorbed water which is bonded by (integrated) van der Waals–London forces; layer B represents the chemisorbed water (water bonded due to dipole-originating Coulomb forces); and layer C represents the chemically bonded OH^- groups (hydroxyl groups). The latter represent the most strongly bonded, potential water. When hydroxyl groups desorb, two combining to form one water molecule (at $T > 375\,^\circ$C [7]), they leave behind two types of surface site: a positively charged aluminium atom with an acid character (Lewis site) and a negatively charged oxygen atom (Brønsted base), both giving the surface distinct chemical properties [4]. The term "active" or "activated" alumina has been used for the transition aluminas due to their capability of catalysing certain chemical reactions and chemisorbing a variety of molecular and ionic species.

4. Degassing

During atomization of aluminium, irrespective of the atomization atmosphere, an amorphous oxide film on the surface of the particles is formed instantaneously

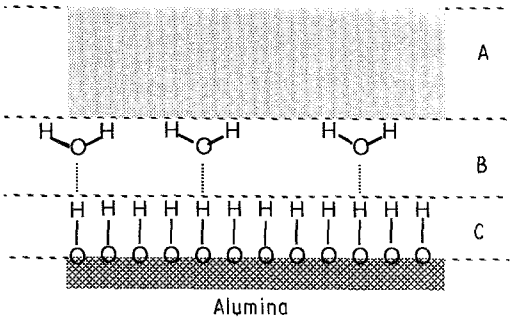

Figure 3 Schematic representation of adsorbed water on a hydrated crystalline alumina surface (see text for explanation).

due to the high affinity of aluminium towards oxygen. As mentioned above, the resulting oxide layer is prone to uptake of moisture from the atmosphere both by chemical and physical adsorption and by chemical reaction (formation of hydroxides).

Annealing in vacuum or inert gas atmospheres drives off the adsorbed gaseous species (volatiles), causes dehydration of the hydroxides and will ultimately result in transformation of the surface layer into crystalline γ-oxide. Annealing in an inert gas as compared to that in vacuum, improves the resistance to rehydration and readsorption of moisture during subsequent exposure to humid air [8]. Vacuum annealing combined with intermittent inert gas flushing can make degassing more effective and more stable to readsorption [9].

Dehydration of the surface hydroxide layer on aluminium powder particles occurs through a progressive series of transformations with temperature. The modifications of the aluminium hydroxides can be envisaged as $Al_2O_3 \cdot xH_2O$, although this representation is structurally incorrect because no lattice water is contained by the pure hydroxides. The following dehydration scheme [10] involving stabilities and reaction temperature ranges, is widely quoted in studies of degassing

$$\underset{150\,^\circ C}{Al_2O_3 \cdot 3H_2O} \xrightarrow{175-310\,^\circ C} \underset{310-500\,^\circ C}{Al_2O_3 \cdot H_2O} \xrightarrow{530-550\,^\circ C} \underset{600-900\,^\circ C}{\gamma\text{-}Al_2O_3} \qquad (9)$$

Owing to the availability of metallic aluminium, part of the water liberated in these series of degassing reactions is converted to hydrogen through Reaction 3.

Ackermann *et al.* [12] have found for air-atomized 7XXX series P/M alloy that three peaks in their hydrogen mass spectrum obtained during vacuum degassing are irreversible and highly temperature dependent. A fourth peak in their hydrogen spectrum (at ~ 400 °C) coincides with a release of metallic zinc and was expected to represent an increase in intensity of interaction of water with the metal, interpreted as a break-up of the oxide layer.

Besides precluding material defects due to trapped hydrogen, degassing of aluminium powders is desirable for obtaining good powder particle bonding during densification: the amorphous oxide layer is transformed into a brittle oxide layer which can be broken and redistributed during consolidation processing. Furthermore, if correctly applied, degassing will lower the oxide content relative to the non-degassed powder by the removal of H_2O [12]. This may lead to a better break-up and dispersion of the brittle layer by minimization of its thickness.

During vacuum degassing of metal powder compacts, the compact density, pore size and permeability are important factors affecting the overall rate of outgassing of the sample.

5. Experimental methods

The density of the fibre was determined with helium pycnometry. Nitrogen gas adsorption/desorption (static volumetric method) was used to determine pore size, porosity and surface area of the Saffil RF alumina fibre. Thermogravimetric analysis (μ-TGA) was performed for the determination of the amount of extractable water contained by this porous fibre. Vacuum degassing was applied to the powder compacts with 0 (ASCM20 only), 5, 20 vol % fibres and to a sample of 100% fibres (fibres only). During these experiments the partial pressures of the evolving gases were recorded as a function of time and temperature. Hydrogen measurements of the powder samples were made using solid extraction. This provides, together with TGA data, additional information to the semi-quantitative gas evolution data. Analyses of oxide content were performed by means of high-temperature reduction with carbon. These analyses were done on the ASCM20 only, which had experienced similar processing to the composite powders because the analysis was not possible for the composite material (containing large volumes of oxidic reinforcement).

5.1. Helium pycnometry

The apparatus used for determination of the density of the fibre material (i.e. density of a solid, excluding the volume of interconnected pores) was a Micromeritics Autopycnometer model 1320. The resulting value of density, the true density, ρ_{true}, is the density of the solid part of the material including the fraction of single and non-interconnected pores. Prior to the analysis, specimens are kept at 150 °C for 17 h. The sample is then weighed and brought into the sample cell, followed by evacuation to $p = 0.1$ mm Hg. The sample cell and a reference cell are filled with equal amounts of helium. The gas in the sample cell will be slightly more compressed owing to the volume taken in by the solid. By a stepwise decrease in the volume of the reference cell until the pressure equals that in the sample cell, the true volume of the specimen is determined. Additional measurements are done after evacuation of the sample cell for 2 h.

5.2. Nitrogen gas adsorption/desorption measurement

The pore size, porosity and specific surface area of the alumina fibre were determined by nitrogen gas adsorption/desorption measurements with a Micromeritics Digisorb 2600. In this instrument, the sample is contained in a sample holder immersed in liquid nitrogen. In the known free volume of the system, distinct quantities of nitrogen are admitted in a stepwise progression, after each step of which the system with sample is left to equilibrate. The amounts of adsorbed nitrogen are calculated from the measured pressure at standard temperature and the theoretically calculated

pressure values. During desorption, the same procedure is followed backwards. A value for the specific surface area is obtained by applying the BET equation to the measured amounts of adsorbed nitrogen at low relative pressures, where a monolayer coverage of the surface is not exceeded.

5.2.1. Calculation of pore size from nitrogen desorption measurements [7]

In the study of pore-size distributions by measurement of nitrogen adsorption, a classification of pores is made according to size, in which macropores are those with diameter $D > 50$ nm; mesopores are those in between 2 and 50 nm; and micropores are those smaller than 2 nm. The calculation of sizes of mesopores from nitrogen desorption data requires the assumption of a pore geometry. Assuming cylindrical pore shape, the (corrected) Kelvin equation, relating the radius of a pore, r_K, in which condensation occurs to the relative pressure, p/p_0, is

$$r_K = \frac{-2\gamma V_{mol}}{RT_b \ln(p/p_0) + F(\tau)} \quad (10)$$

where γ is the surface tension of nitrogen at its boiling point (0.885 J m^{-2} at 77 K), V_{mol} is the molar volume of liquid nitrogen at its boiling point (34.7×10^{-6} m^3 mol^{-1}), R the gas constant, and T_b the boiling point of nitrogen (77 K). The function $F(\tau)$ is a correction term applied to the original Kelvin equation and takes into account the dependence of the chemical potential of the adsorbate on the adsorbed layer thickness, τ. Because prior to condensation some adsorption will take place in the pores, this adsorbed layer thickness, τ, is to be incorporated in Equation 10 to define the actual pore radius

$$r_p = r_K + \tau \quad (11)$$

The statistical τ can roughly be considered as 0.354 V_a/V_m in which 0.354 nm is the thickness of one nitrogen molecular layer, and V_a/V_m is the ratio of the volume of nitrogen truely adsorbed at a given relative pressure to the volume adsorbed at the completion of a monolayer, both for a non-porous solid of the same composition as the porous sample. The curve of p/p_0 versus τ (for nitrogen) appears to be similar in shape for a number of materials. Therefore, a general curve can be derived which is called the "common τ-curve", representing the standard nitrogen adsorption isotherm per unit of surface area. It is used to obtain values for τ as a function of p/p_0. For materials exhibiting τ-type adsorption behaviour, the function $F(\tau)$ is derived from this common τ-curve using $F(\tau) = -RT\ln(p'/p_0)$. The pore-size distribution may be derived by combination of the experimental desorption isotherm and Equations 10 and 11.

5.3. Thermogravimetry

Thermogravimetric experiments were performed with the fibre material in a Stanton Redcroft TG-770 micro-balance. To prevent take-up of moisture, an atmosphere was selected consisting of a flow of nitrogen (99.9% pure) of 15.75 $l\,h^{-1}$. An annealing atmosphere consisting of flowing purified nitrogen may accelerate degassing [9]. Comparison with a continuously pumped vacuum atmosphere in this context is not unrealistic. The nitrogen was filtered for extraction of oxygen and H_2O. Samples of ~ 10 mg fibres were weighed in a platinum cup. A heating rate of 10 °C min^{-1} and subsequent free cooling in the flow of nitrogen were employed. Owing to the decrease of gas density with rise in temperature, it was necessary to correct the curves for the loss in buoyancy force (causing a positive Δm term). For this reason, a baseline was derived with a sample of fused alumina (low specific surface) of the same weight as the fibre sample.

5.4. Degassing

Fig. 4 shows a schematic drawing of the experimental apparatus used for degassing. The quadrupole mass spectrometer (QMS) installed is an Edwards EQ 80F. The apparatus is capable of measuring gaseous species with masses up to atomic mass units (a.m.u.) of 80, presenting the data in pressure units.

Powder was cold-precompacted in aluminium cans of 6063 alloy (Al–0.4Si–0.7Mg) to relative densities of ~ 0.60 (Table III) for matrix and composites and to 0.15 theoretical density for the sample of fibres only. A cover and tube were welded to each of the cans. This presented some problems in the stage of final closure due to expansion of gases inside the can, blowing open the weld bath. Once hermetically closed, a can was connected to the degassing line (Fig. 4). A sintered bronze filter was positioned at the end of the tube to restrict contamination of the system with powder. The following samples were degassed (Table III); one can containing no material; one containing ASCM20 only; cans containing composites with 5 and 20 vol %, and one can containing an amount of fibres only equal to that in the can with the 20 vol % composite.

After pumping the system to a prevacuum of $\sim 10^{-5}$ bar, the turbomolecular pump (TMP) was activated and left to pump until a system pressure of $\sim 10^{-9}$ bar was reached. This was done to guarantee continuous operation of the QMS within the required low-pressure range. The pumping times to reach this pressure (during which the samples are undergoing room-temperature degassing) vary among the different samples from 1–10 h. After reaching the starting vacuum, the experiment was initiated by heating the can at 2.5 °C min^{-1} to ~ 550 °C. The mass spectrum of the pumped gases was measured every fifth minute at

TABLE III Masses and porosities of vacuum-degassed materials

Material/V_f	m(ASCM20) (10^{-3} kg)	m(fibres) (10^{-3} kg)	Compact porosity, Ω
Empty can	–	–	–
ASCM20 only	290.2	–	0.41
0.05	272.33	17.07	0.40
0.20	222.53	70.27	0.41
Fibres only	–	69.33	0.85

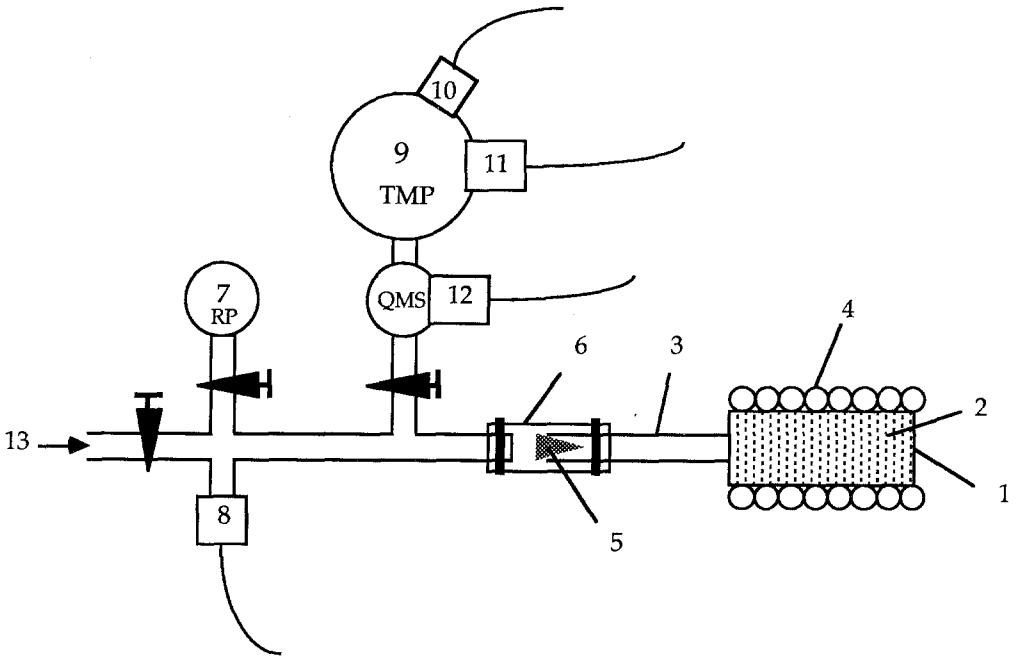

Figure 4 Schematic drawing of experimental degassing line. 1, can; 2, powder compact; 3, tube welded to can; 4, furnace; 5, bronze filter; 6, brass coupling with O-rings; 7, rotary pump (pre-vacuum); 8, Pirani meter; 9, turbo-molecular pump with 10, Pirani meter and 11, Penning meter; 12, quadrupole mass spectrometer; 13, flushing gas insertion point.

a.m.u.s of 2 (H_2), 4 (He), 18 (H_2O), 28 (N_2/CO), 32 (O_2), 40 (Ar) and 44 (CO_2).

The present experimental apparatus comprises a so-called differential pumping whereby one part of the vacuum system is maintained at a higher vacuum (QMS chamber) than another (e.g. can interior) because of diametrical restrictions (a.o. filter) in the tubings. The pressure in the can during analysis is estimated to be of the order of 10^{-6}–10^{-7} bar.

Studies of vacuum degassing may be undertaken with the aim to derive workable parameters for isothermal process degassing of a specific material. This target was beyond the scope of the present research.

5.5. Hydrogen analysis

The initial amounts of hydrogen in the powders were measured by the method of hot solid extraction. The apparatus used was a Ströhlein H-mat 251 hydrogen gas analyser. The method uses the change in conductivity due to hydrogen of a carrier gas, in this case nitrogen. The analysis was performed as follows: A sample of ~ 2 g powder was weighed in a quartz spoon and transferred to a furnace at 550 °C. Each measurement lasted 20 min, after which the signal had died away. The microprocessor calculated the hydrogen level (in p.p.m. by weight).

Water at the surface of the powder is expected to convert to hydrogen according to Reaction 3. The temperature of the analysis is above the solidus of 507 °C of the as-atomized alloy as determined by DSC [13]. It was chosen at this level to obtain a high activity of Reaction 3 and a high hydrogen mobility. Errors in the analysis due to increased hydrogen solubility in the (small) melt fraction are thought to be insignificant, firstly because the major part of the hydrogen will evolve from moisture at the surface of the powder, and secondly because the continuous removal of the released hydrogen in the nitrogen gas stream provides an out-of-equilibrium condition, thereby driving off the major part of hydrogen in the sample.

The present method of measuring hydrogen in solid aluminium is not very general. This is because reproducibility is affected by factors such as sample preparation method, sample thermal history, temperature of analysis and temperature and heating rate during analysis, all relating to the character of hydrogen in aluminium. Therefore, these factors need to be carefully controlled. In the case of powders, where the major part of detected hydrogen originates from the surface oxide layer, even larger uncertainties may be involved due to increased interaction with the atmosphere. Comparison of absolute values between different series of data amongst which factors above could have changed, should be done with a cautious mind.

5.6. Oxygen analysis

This analysis was performed to assess the influence of milling (time) during the applied ball-milling/mixing process on the oxygen content. During the process, oxygen might be incorporated both by Reactions 1 and 3 as well as by increased adsorption. The analysis is such that adsorbed oxygen in any form will be taken into account.

A Ströhlein OSA-mat 350 was used. With this equipment oxygen is analysed in metals and other solids by means of reduction with carbon at very high temperatures

$$MeO(s) + C(s) \rightarrow Me(s) + CO(g) \qquad (12)$$

The carbon monoxide concentration in the carrier gas argon is measured using an infrared spectrometry

technique. The microprocessor converts the data in weight per cent of atomic oxygen. Continuous recording of detected oxygen against temperature is also possible, resulting in an oxygen spectrum. The apparatus was used in the continuous heating mode, whereby the sample was heated from 1000 °C to 2400 °C in ~ 100 s.

Powder samples of 0.050–0.100 g were weighed in small nickel containers of ~ 0.180 g. The nickel serves to prevent severe contamination of the apparatus due to metal evaporation and results in better reproducibility of the data.

6. Results

6.1. Helium pycnometry

In Table I, the results of density determinations and calculations on the Saffil fibre are also displayed. The density of the material obtained in the pycnometric analysis at first seems to correspond to the range of values given by ICI [3]. However, the presently determined value is not a fibre density but a true material density; the fibre density is lower due to the porosity present (see below). Using the producer's value of its pore volume (Fig. 1), together with the true material density, $\rho_{true,exp}$ (see Table I), we can calculate a fibre density, i.e. all-over density, ρ_f, of the fibre

$$\rho_f = 1 \Big/ \left[\left(\frac{1}{\rho_{true,exp}} \right) + V_p \right]$$

$$= 10^3 \Big/ \left[\left(\frac{1}{3.52} \right) + 0.073 \right] \text{kg m}^{-3}$$

$$= 2.80 \times 10^3 \text{ kg m}^{-3} \quad (13)$$

The porosity of the fibre is found from

$$\Omega = V_p \rho_f$$

$$= 0.073 \times 2.80$$

$$= 0.20 \quad (14)$$

The above value of ρ_f notably differs from density values stated by the manufacturer ($3.3–3.5 \times 10^3$ kg m^{-3}). The latter values may not take into account open porosity. One consequence of this porosity is that the present materials (prepared assuming a density of 3.3×10^3 kg m^{-3}) have actual volume fractions in excess of the target values of V_f of 0.05 and 0.20. The correct values V_f^*, assuming validity of the values in Equation 13, are 0.056 and 0.228, respectively, and will be applied below only when relevant.

6.2. Nitrogen adsorption/desorption

Fig. 5 shows the adsorption and desorption isotherms of Saffil Milled. A considerable hysteresis effect is present indicating capillary condensation in pores. At low pressures an amount of gas is quickly adsorbed after which the adsorption is relatively invariable to pressure. This, and the fact that the hysteresis loop does not close during desorption before reaching a relative pressure, p/p_0, of 0.3, points to the presence of micropores [7]. These small pores cannot be determined by the present method and are therefore not included in the pore-size distribution given in Fig. 6. This size distribution is calculated with desorption data of $0.43 < p/p_0 < 0.79$ assuming a cylindrical pore geometry. A value for the pore volume, $V_p = 0.045 \times 10^{-3}$ m^3 kg^{-1}, not accounting for micropores, was obtained from the analysis.

6.3. TGA

In Fig. 7 the results of the TGA analysis on the Saffil fibre are displayed. Two heating and free cooling cycles were given to the sample. After the first heating to 560 °C, the sample of 0.0102 g had lost a mass of

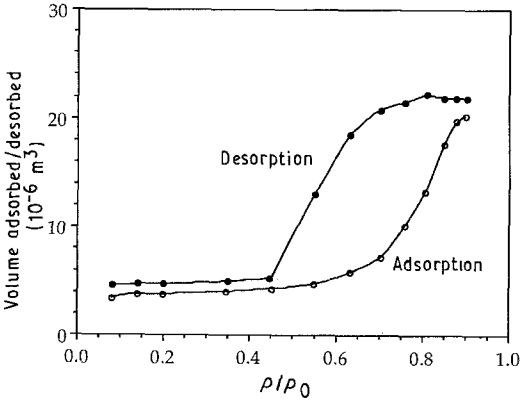

Figure 5 Nitrogen (○) adsorption and (●) desorption isotherms for Saffil Milled fibre.

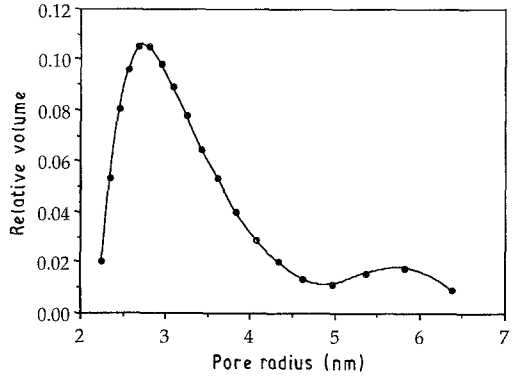

Figure 6 Mesopore-size distribution of Saffil Milled fibre derived from nitrogen desorption data.

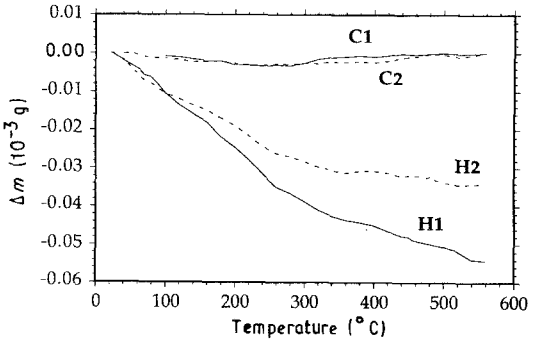

Figure 7 Results from μ-TGA analyses on Saffil Milled fibre. H1 and H2, C1 and C2 are first and second heating and cooling, respectively. Heating rate 10K min^{-1}, free cooling, fibres only, $m = 10.2 \times 10^{-3}$ g.

0.054×10^{-3} g. After an initial constant rate of mass loss, a decrease occurred at $T \sim 260\,^{\circ}C$.

After the first cooling to room temperature (in the graph Δm, at $T = 560\,^{\circ}C$, was set to 0) the weight remains unchanged. A small decrease can be observed in cooling to 260 °C which, however, is compensated again on further cooling to room temperature.

A second heating (Δm, at $T = 20\,^{\circ}C$, was set to 0) results in an additional decrease in weight. Again, no net weight change takes place during cooling which also indicates that within the time span of the cooling, no relevant adsorption of nitrogen takes place. The total loss of mass in these two runs was 0.088×10^{-3} g which amounts to 0.86 wt % . Attributing this weight loss to molecular water results in a potential hydrogen (weight) content of 0.0956% = 956 p.p.m.

6.4. Degassing

Below, some consideration on the relevance of the QMS recordings (the degassing curves) will be given before presenting them.

Because of the high vacuum in the analysis chamber (in which the QMS is installed) it may be justified to regard gases in this part of the system with the ideal gas law, noting, however, that the number of molecules in the analysis chamber, n, is varying with time. Thus

$$p = \frac{nRT}{V} \tag{15}$$

with T and V for this part of the system being constant, giving

$$p = K_1 n \tag{16}$$

The pressure is proportional to the number of molecules in the analysis chamber. When the QMS detects a change in pressure, it will be due to a change in the number of molecules

$$\left(\frac{dp}{dt}\right) = K_1 \left(\frac{dn}{dt}\right) \tag{17}$$

where

$$\left(\frac{dn}{dt}\right) = \left(\frac{dn_a}{dt} - \frac{dn_e}{dt}\right) \tag{18}$$

and in which dn_a/dt is the arrival rate of molecules in the analysis chamber and dn_e/dt is the evacuation rate of the molecules through discharge by the TMP.

In the interpretation of the degassing curves it will be assumed that the relative rate of liberation of gas molecules from the powder surface (dn_1/dt) is proportional to the arrival rate of molecules in the analysis chamber

$$\left(\frac{dn_a}{dt}\right) = K_2\left(\frac{dn_1}{dt}\right) = K_2\left(\frac{dT}{dt}\frac{dn_1}{dT}\right) \tag{19}$$

in which dn_1/dT is determined by thermodynamic and kinetic factors, and dT/dt is the heating rate of powder in the can. Owing to the high-vacuum conditions in the system a phase difference between degassing event and the corresponding QMS signal detection is not expected to be significant.

Thus, changes in pressure are related to changes in the fluxes of molecules evolving from the powder (Table IV). Extrema in the curves ($dp/dT \simeq dp/dt = 0$) represent stages where the rates of arrival and evacuation of the molecules are the same. Inflexion points ($d^2p/dT^2 = 0$) on negative slopes represent the stages at which the flux of molecules arriving is at a minimum; at these points new degassing events take off.

6.4.1. Water

Fig. 8 shows the QMS curves of H_2O pressure during degassing grouped together. In heating up towards 100 °C all the materials except the empty can display a sharp increase in H_2O pressure. In this stage, apparently one or more H_2O releasing processes start to take place that are typical for the powders.

The curves of ASCM20 only and composite with $V_f = 0.05$ are fairly undulating (e.g. maxima for the latter at 220, 300, 380 and 450 °C) which is not the case for the curves of $V_f = 0.20$ and fibres only. The extrema are more pronounced in the case of the composite.

The high H_2O pressures as found above 100 °C are maintained up to increasingly higher temperatures with increase in V_f from 0 to 0.20. The intensive water liberation is either extended towards higher temperatures, or shifted up in time for materials with higher fibre volume fractions.

The sample of fibres only shows a similar evolution up to 250 °C as compared to the material with $V_f = 0.20$. After that, the water pressure of the fibres only sample slowly drops up to a temperature of

TABLE IV Significance of the shapes of the degassing curves

$\frac{dp}{dT} = 0$	Pressure constant, gas supply rate = evac. rate
$\frac{dp}{dT} > 0$	Pressure increase, gas supply rate > evac. rate
$\frac{dp}{dT} < 0$	Pressure decrease, gas supply rate < evac. rate

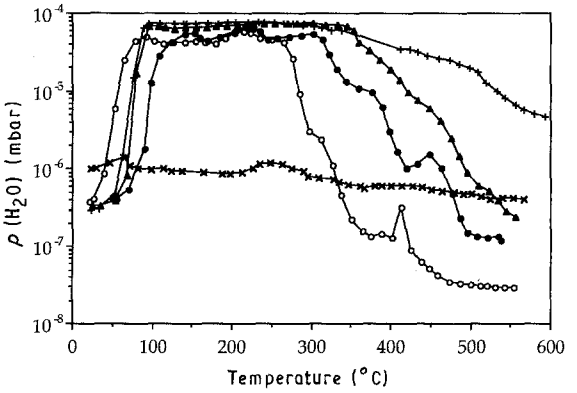

Figure 8 Water mass spectra recorded during vacuum-degassing experiments at 2.5 °C min^{-1}. (×) Empty can, (○) ASCM20 only, (●) $V_f = 0.05$, (▲) $V_f = 0.20$, (+) fibres only.

500 °C, whereas for the composite the decay of $p(H_2O)$ takes place much more rapidly than for the fibres only.

6.4.2. Hydrogen

Fig. 9 illustrates the QMS signals from hydrogen. Heating up to 100 °C again shows a drastic rise of pressure for all materials but the empty can. In this stage the quotients of $p(H_2)/p(H_2O)$ remain more or less constant at 0.01.

The hydrogen pressure of the ASCM20 only sample falls off at a temperature of 285 °C after a steady rise from 100 °C. This follows shortly after the drop in H_2O pressure (Fig. 8). After this, the pressure only rises slowly until it sharply increases at 400 °C. The corresponding peak at ~ 415 °C is very acute.

The curves of 5 and 20 vol % show a more or less continuous rise of $p(H_2)$ up to 450–475 °C. In the former curve a minimum is formed at 410 °C and a broader peak at 450 °C. The curve of the 20 vol % composite is relatively flat-topped with a maximum located at 478 °C. It is noted that the drops in H_2O pressure as found at 265 and 310 °C for the 5 and 20 vol % composites, respectively, are not reflected in the hydrogen pressure curves. A small rise in signal of the 20 vol % curve is noticed only at 350 °C. Apparently, there is a continuous supply of H_2O from within the powder to feed the hydrogen-producing Reaction 3.

The hydrogen pressure in the fibres only specimen follows the initial rise below 100 °C after which it remains more or less constant up to 450 °C, where it again rises steeply.

6.4.3. Oxygen

Fig. 10 gives the oxygen signals during degassing. A rapid decrease in oxygen pressure in the ASCM20 only sample occurs at 265 °C. The composites also show a sudden decay of pressure at temperatures in the range 240–270 °C. However, the rate of pressure loss becomes lower with increasing fibre content while for the fibres only sample the pressure decreases more or less exponentially from 100 °C upwards.

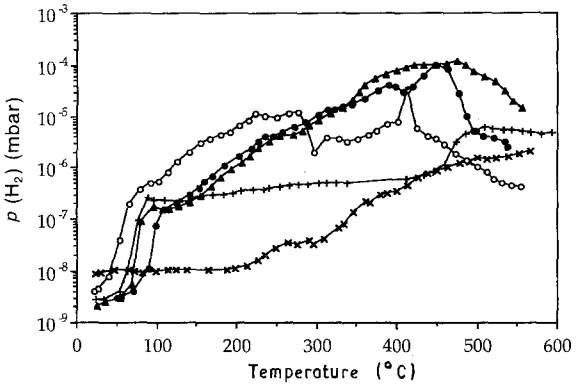

Figure 9 Hydrogen mass spectra recorded during vacuum-degassing experiments at 2.5 °C min^{-1}. (×) Empty can, (○) ASCM20 only, (●) $V_f = 0.05$, (▲) $V_f = 0.20$, (+) fibres only.

6.5. Hydrogen analyses

Fig. 11 presents the results of the analysis of hydrogen in samples of milled powder ASCM20 only. The influence of two operation modes of the ball mill (both used for the preparation of the present composites) has been tested. A low-speed (cascading [14]) operation applied in the preparation of composite with $V_f = 0.20$ results in a small rise in hydrogen content with milling time. The high-speed operation (applied during preparation of composites with $V_f = 0.05$) corresponding to a more intense batch motion (cataracting [14]) causes a relatively sharp increase during the initial 10 min milling. It is noted that the relative amounts of hydrogen uptake are very small. The difference in the pattern of hydrogen uptake between the two operation modes can be explained by differences in equilibration of the powder surface with moisture in the mill drum because of different mixing rates.

The hydrogen contents of the composites are given in Fig. 12. Cross-hatched bars represent the mean of two samples from one powder production batch. The second bars represent averages of two to three different batches. The hydrogen level increases with increase in V_f. It is not clear why, for the 5 vol % composite, the same value is found as for the ASCM20 only sample after similar processing. Furthermore, hydrogen contents of the composites as measured are not as high as expected on the basis of TGA-derived

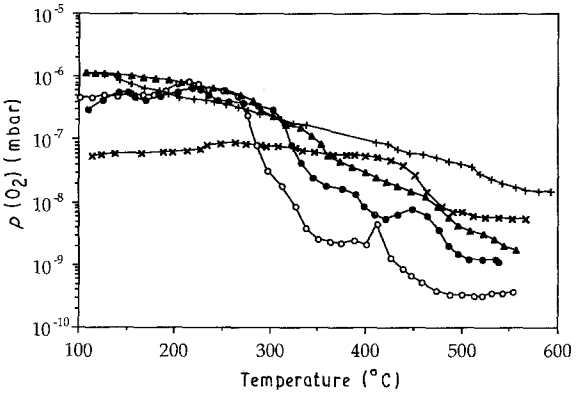

Figure 10 Oxygen mass spectra recorded during vacuum-degassing experiments at 2.5 °C min^{-1}. (×) Empty can, (○) ASCM20 only, (●) $V_f = 0.05$, (▲) $V_f = 0.20$, (+) fibres only.

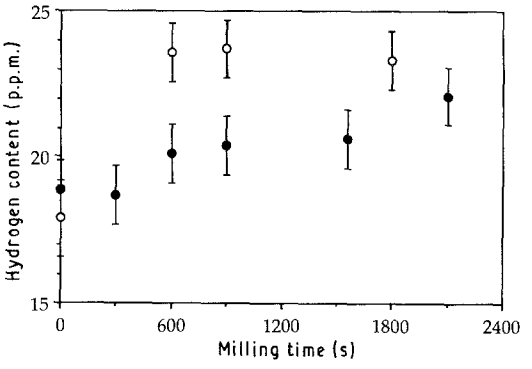

Figure 11 Results of hydrogen analyses by solid extraction of milled ASCM20 only; hydrogen content versus milling time at (●) 60–65 r.p.m, (○) 110 r.p.m.

TABLE V Comparison of data from hydrogen solid extraction analyses with calculated hydrogen contents of composite powders using TGA data on fibres (see text)

V_f	Hydrogen content (p.p.m.)		Hydrogen fraction exp.
	(experimental)	(calculated)	detected
ASCM20-only	18	–	–
milled	23	–	–
0.05	22	76	0.29
0.10	29	132	0.22
0.20	41	245	0.17
Fibres only	956[a]	–	–

[a] From TGA analysis.

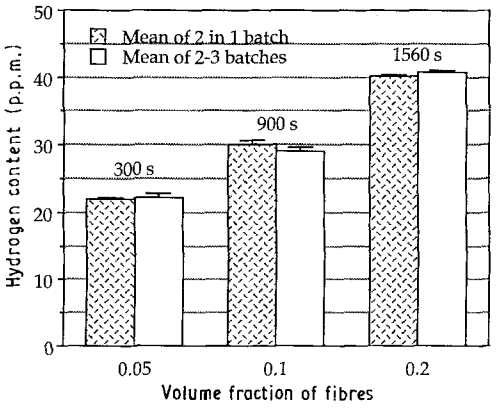

Figure 12 Results of hydrogen analyses by solid extraction of composites: applied milling times are indicated.

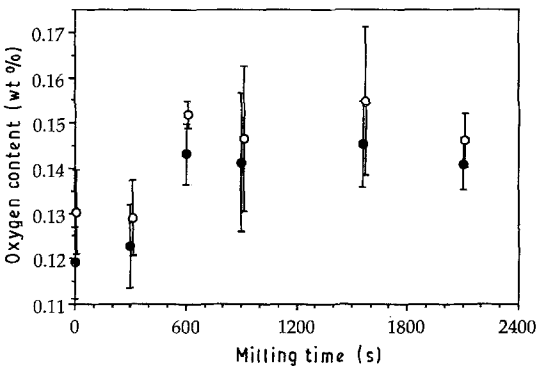

Figure 13 Results of oxygen analyses of ASCM20 only as a function of milling time. (●) Higher oxides, (○) total.

water contents of the fibres only sample (Table V). It appears that the detected fraction of total hydrogen decreases with increasing V_f.

6.6. Oxygen analyses

The influence of milling time on oxygen content of the ASCM20 only powder is illustrated in Fig. 13. One curve represents the total amount of oxide while the other gives the fraction of the so-called higher oxides (of aluminium and magnesium, melting at $T > 2000\,°C$). A small increase in oxygen content takes place in the first 10 min milling (at low speed, 60–65 r.p.m.). The final oxygen content of 0.15 wt % [O] is equivalent to a weight fraction of Al_2O_3 of approximately 0.31 wt %, which is taken as a lowest estimate for the matrix in the present composites in the pre-degassing stage. During outgassing of the composites, Reaction 3 may, at the most, increase the oxide content (of the matrix!) to a value of 0.5 wt % for the composite with $V_f = 0.10$ and to 0.8 wt % for the matrix in the material with $V_f = 0.20$.

7. Discussion

7.1. Density and specific surface of Saffil fibres

A density for the Saffil fibre of 3.52×10^3 kg m^{-3} was determined by helium pycnometry (Table I). The value is lower than the value of 3.69×10^3 kg m^{-3} for the true density of the orthorhombic δ-alumina, which can be calculated from the unit-cell dimensions (see Appendix A.2). The discrepancy may be attributed to closed porosity and/or to the partly amorphous nature (79% crystallinity) which will cause a slightly less dense material. The 4 wt % silica added may also cause a small density decrease.

With the pore volume, V_p, and mean pore size, d_p (assuming cylindrical pore shape), a specific surface, S_p, of the fibre can be calculated as follows

$$S_p = \frac{4}{d_p} V_p \qquad (20)$$

Taking the experimentally determined values of $V_p = 0.045 \times 10^{-3}$ m^3 kg^{-1} and $d_p = 6$ nm (Table I) and using Equation 20 one should expect a value which underestimates the actual surface area due to the simplicity of the cylindrical pore model. Still, the value of $S_p = 30 \times 10^3$ m^2 kg^{-1} derived in this way is nearly twice that experimentally obtained (BET method with nitrogen). It should also be realized that the true specific surface of the fibre (i.e. the surface which can be acted upon by the smallest volatile species, e.g. helium, hydrogen and possibly OH^- groups) could be significantly higher than 16.8×10^3 m^2 kg^{-1}.

7.2. Water in Saffil fibres

As we have seen above, sources of water evolving from the fibres at elevated temperature include chemisorbed water, which is typically a monolayer adsorption, and physically adsorbed water, which involves adsorption in multilayers. Chemically adsorbed water

molecules can desorb at low temperature ($T < 127\,^{\circ}C$ [4]) while desorption of hydroxyl groups (a process with high activation energy [15]) only occurs rapidly at high temperatures ($T > 375\,^{\circ}C$). For the present Saffil material, it is calculated that complete desorption of such a hydroxyl monolayer results in a mass loss of 0.26 wt % (Appendix A.1). Peri and Hannan [15] have found by means of infrared spectroscopy that desorption of the hydroxyl layer on γ-alumina is a slow process and does not go to completion even after heating at $\sim 1000\,^{\circ}C$.

Physical adsorption of more than one layer in porous materials can be continuous with the process of capillary condensation (see Section 5.2.1). The kinetics of physical adsorption occur with an activation energy of zero, as is also the case with condensation due to van der Waals–London forces. This implies that adsorption and desorption rates on flat surfaces can be very high. However, for material with a very fine pore structure, as in the present fibre, it is likely that the desorption step at the (internal) surface is not the rate limiting factor in the release of water, but that diffusional removal of the water out of the pore structure may be so.

Given the total specific pore volume of the fibre material of $0.073 \times 10^{-3}\ m^3\,kg^{-1}$ (Table I), the maximum possible water content would be 7.3 wt %. An amount of 0.86 wt % is experimentally found which corresponds to a volumetric pore filling of ~12%. In cylindrical pores of the same size this would mean a fill of a volume segment with a thickness of 6% of the pore radius. However, very fine pores are also present which implies that some of them may be completely filled with moisture.

A first stage in the degassing curves of the fibres only sample (Stage I, Fig. 14) is explained by a large inequality between the rate of gas evolution due to rapid desorption and the evacuation rate, giving rise to a pressure rise in the analysis chamber. In Stage II (up to 260–300 °C), the pressure remains constant, implying that an equilibrium is established between gas evolution and evacuation. It is correlated to the initial event, giving a constant rate of mass loss (up to 260 °C) in the TGA experiment (Fig. 7). A dynamically sustained constant water pressure will have to be maintained in the pores of the fibres. Above 260 °C in the TGA experiment, the rate of mass loss has decreased. A parallel is drawn with Stage III of vacuum degassing (Fig. 14). At that interval, physical desorption will have ceased while chemically adsorbed molecular water will continue to desorb. The latter is thermally activated and is a much slower process than physical desorption.

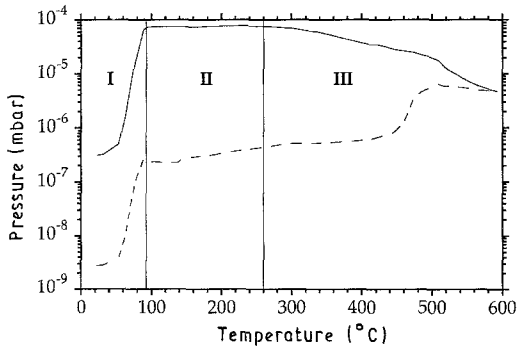

Figure 14 Distinction of three stages in the vacuum degassing of Saffil fibres only, at 2.5 °C min^{-1}. Curves exemplified from Figs 8 and 9. (– – –) $p(H_2)$, (——) $p(H_2O)$

When the degassing curves of the materials with $V_f = 0.05$ and 0.20 are studied closely, the following points can be made. As mentioned above, extrema in $p(H_2O)$ and $p(H_2)$ are clearly present in the curve of $V_f = 0.05$, but are not in that of $V_f = 0.20$. In the latter material the expected complex signal of water from dehydration of the metals' surface hydroxides is most likely obscured by that of large quantities of water continuously evolving from the 20 vol % ceramic fibres.

A large discrepancy was found between the values of hydrogen content of the fibres from solid extraction analyses and that derived from thermogravimetric analyses (Table V). Because the results of the latter method are considered most reliable, it is concluded that in the case of the solid extraction analyses a substantial part of potential hydrogen remains unseen. The argument that, at 550 °C, Reaction 3 at the metal powder surface is incomplete, is unsatisfactory due to the magnitude of the differences. A more plausible scenario might be that such a large amount of water is emerging from the fibres shortly after transfer to the furnace at 550 °C, that the reductive capacity of the metal powder surface is exceeded. This questions the reliability of the solid extraction method for determination of surface hydrogen in these composites.

7.3. Degassing curves

In the $p(H_2O)$ and $p(H_2)$ curves of the ASCM20 only sample and composite $V_f = 0.05$, small undulations are visible. They can be attributed to sudden releases of water due to dehydration reactions in the series represented by Equation 9. The pressure of hydrogen is related to that of water due to Reaction 3. The fact that the peaks in the composite material with $V_f = 0.05$ are shifted and more pronounced may be attributed to a different state of the surface hydroxides on the metal powder, because this material has (unlike the ASCM20 only sample) experienced ball-milling.

Below the decay temperatures of $p(H_2O)$, the patterns of hydrogen evolution in the ASCM20 only sample and composites are similar, exhibiting a steady rise. It most likely represents the increase in activity of Reaction 3 with temperature. It is remarkable to find for the ASCM20 only sample that, whereas the decay of $p(H_2O)$ is followed by a decrease of $p(H_2)$, the latter continues to increase for the composites at the same stages. This indicates that a fraction of the hydrogen does not originate from the metal powder but, consequently, from the fibres.

The curves of detected oxygen pressure can be interpreted in line with the theory of Mott/Wagner [16, 17]. This theory predicts a limiting thickness of 2 nm oxide layer formed on aluminium at room temperature during exposure to air. Above a temperature of

260 °C, this oxidation barrier should break down enabling the oxide layer to continue to grow. In Fig. 10, the curve of the ASCM20 only sample clearly demonstrates a sharp decrease in oxygen pressure. This is attributed to a sudden increase in oxygen consumption by Reaction 1, indicating growth of the oxide layer on the powder. It is noted that with the oxygen pressure, the water pressure also decays. The curves of the composites show a less steep decay of $p(O_2)$. This is attributed to the availability of more water and the competition of Reactions 1 and 3. Therefore, it is concluded that, during the present degassing below 260 °C, oxidation of the matrix does preferentially occur with water through Reaction 3. In the ASCM20 only sample where, above the temperature of 265 °C, a decrease in availability of water occurs, the oxygen at that stage is consumed most quickly. The limit temperature of 260 °C predicted by the Mott/Wagner theory, also appears from the $p(O_2)$ curves of the composites. For these materials the discontinuity is encountered in the range 240–270 °C, providing evidence for the accuracy of temperature control during the experiments.

With the rough assumption that the pumping speed was constant during and amongst the experiments, we may compare the amounts of gases having evolved from the samples by calculating the area below the pressure curves and normalizing with the powder masses. The results of such a calculation for hydrogen and for water are displayed in Fig. 15. It appears that the composites show a depletion in the amount of water with respect to the theoretical linear mixture. However, the values for hydrogen compensate for this lack, showing that indeed water originating from the fibres is converted to hydrogen by oxidation with the metal powder.

8. Conclusions

From gas analyses during experimental vacuum degassing of the present composites (compared to matrix behaviour), sustained high water pressures and delayed peak hydrogen production are found. These are attributed to the presence of the δ-alumina fibres.

The applied Saffil RF Milled fibre has microporosity ($d < 2$ nm) and a pore volume due to pores of size $d > 4$ nm of 0.045×10^{-3} m^3 kg^{-1}. The specific surface of 16.8 m^2 g^{-1} determined by nitrogen adsorption is an underestimation of the true hydroxilized internal surface. In the light of these facts, the high water content of 0.86 wt % is not inexplicable. It is known that physisorbed water (adsorbed in multilayers) constitutes the largest fraction of water on an alumina surface. This is also the fraction that will desorb most easily on heating, with zero activation energy. The present Saffil fibre with its large specific internal surface area, initially releases water at a rate invariable to temperature. This is thought of as condensed and physisorbed water diffusing out of the fine pore spaces. After some time the dewatering rate drops, which is attributed to the completion of physical desorption.

Hydrogen analyses (solid extraction method) of the 0, 5, 10 and 20 vol % powders before degassing show an increase with increase in fibre volume fraction and a weak dependence on applied powder mixing (milling) time. The hydrogen contents (mainly due to surface moisture) are gross underestimations of the amounts inferred from thermogravimetry on the fibres. This is attributed to the incompleteness of Reaction 3 caused by excess H_2O at the reactive metal surface during incipient heating.

The decay of water pressure at 265 °C during the present degassing of the ASCM20 only sample corresponds to a decay in oxygen pressure and may be interpreted according to the Mott/Wagner theory of oxidation of aluminium. It is due to breakdown of the protective nature of the oxide/hydroxide film of the underlying metal surface towards oxidation by oxygen. Below 265 °C, the protective capacity towards oxidation by oxygen is constant, whereas the activity of the reaction with water, as monitored by the hydrogen pressure, increases.

Relative to the matrix material, the composite with a fraction of fibres as low as $V_f = 0.05$ contains more water. Correct degassing of these composites, therefore, requires effective degassing of the matrix as well as the fibres. Because of outward diffusional transport being slow from a fine-porous material, time is an important factor to be taken into account for degassing of the fibres, whereas temperature, in turn, is the key factor to be considered for complete dehydration of the metals surface oxide/hydroxide film. Thus, for these composites, the parameters for optimum degassing are more confined than for the single constituents.

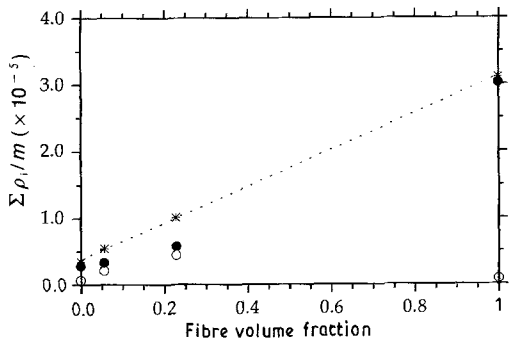

Figure 15 Areas under degassing curves of (●) water (Σ_p (H_2O)) and (○) hydrogen (Σ_p (H_2)) normalized by mass, m, as relative indicators of quantities released during degassing (*) Sum.

Acknowledgements

The authors are indebted to Professor B. M. Korevaar for his critical review and stimulating discussions. The financial support from the Foundation for Technological Research (STW) and the Foundation for Fundamental Research of Matter (FOM) is gratefully acknowledged.

Appendix

A.1. Derivation of weight fraction of surface hydroxyl groups on α-Al_2O_3

With the assumption that all of the internal surface of the fibre is along the densest crystallographic plane

(0 0 1), this gives, with 2 atoms per base of the unit cell, a surface occupation of 2 aluminium atoms per $a^2 \sin(180\text{-}\gamma) = (0.4759)^2 \sin 60° = 0.19614\ nm^2$. Combining this with the experimentally determined specific surface area of $16.8 \times 10^3\ m^2\ kg^{-1}$ makes a number of 1.7131×10^{20} aluminium surface atoms per gram Al_2O_3. When all these surface atoms are bonded 1:1 to hydroxyl groups, this will yield 0.0049 g OH/g Al_2O_3. Transforming this into a pure oxidic surface requires the combination of two hydroxyl groups to form one water molecule [4]. Accordingly, an amount of $18/34 \times 0.0049 = 0.0026$ g H_2O/g $Al_2O_3 = 0.26$ wt % H_2O is found that may theoretically evolve from complete dehydroxilation of the surface layer.

A.2. Calculation of theoretical (true) density of δ-Al_2O_3

Taking orthorhombic crystallography for the δ-phase of alumina, and cell parameters of $a = 0.425$ nm, $b = 1.275$ nm, $c = 1.021$ nm [4], the unit cell containing 12 molecules has a volume of 0.5533 nm^3. This amounts to a theoretical density of $3.69 \times 10^3\ kg\ m^{-3}$.

References

1. B. FUBINI, M. VOLANTE, V. BOLIS and E. GIAMELLO, *J. Mater. Sci.* **24** (1989) 549.
2. J. H. TERHAAR and J. DUSZCZYK, *ibid.* **26** (1991) 3628.
3. DATASHEET SAFFIL, ICI, RUNCORN, UK. (1988).
4. K. WEFERS and C. MISRA, "Oxides and Hydroxides of Aluminium", Alcoa Technical Paper 19 (Alcoa, 1987).
5. I. L. ROIKH, N. A. LITOVCHENKO, S. G. BELITSKAYA, O. F. GUSAREVA, A. S. SAKHIEV, A. B. BASSEL and L. T. EGOROVA, translated from *Poroshkovaya Metallurgiya* **165** (1) (1976) 56.
6. A. NYLUND and I. OLEFJORD, *Mater. Sci. Eng.* **A134** (1991) 1225.
7. J. J. F. SCHOLTEN, Reader Katalyse en Katalysatoren (st56), Chemical Technology Department, T. U. Delft, The Netherlands (1985).
8. L. A. ARBUZOVA, V. A. DANILKIN and L. L. KUNIN, translated from *Poroshkovaya Metallurgiya* **165** (9) (1976) 1.
9. J. L. ESTRADA-HAEN and J. DUSZCZYK, *J. Mater. Sci.* **26** (1991) 3909.
10. A. L. LITVINTSEV and L. A. ARBUZOVA, translated from *Poroshkovaya Metallurgiya* **49** (1967) 1.
11. M. J. STARINK, V. JOORIS and P. VAN MOURIK, in "Proceedings of the ASM Conference on Heat Treatment and Surface Engineering", 22–24 May, 1991, Amsterdam. edited by E. J. Mittemeijer, *Trans. Tech. Publ.* pt. 1, (1992) 85.
12. L. ACKERMANN, I. GUILLEMIN, R. LALAUZE and C. PIJOLAT, in Proceedings of TMS-AIME Symposium on "Aluminium Powder Metallurgy", Toronto, October 1985, edited by G. J. Hildeman and H. J. Koczak (TMS–AIME, Warrendale, PA, 1985 p. 135).
13. Y.-W. KIM, W. M. GRIFFITH and F. H. FROES, *J. Metals* August (1985) 27.
14. J. H. TER HAAR and J. DUSZCZYK, *Mater. Sci. Engng* **A135** (1991) 65.
15. J. B. PERI and R. B. HANNAN, *J. Phys. Chem.* **64** (1960) 1526.
16. L. KOWALSKI, B. M. KOREVAAR and J. DUSZCZYK, *J. Mater. Sci.* **27** (1992) 2770.
17. N. CABRERA and N. F. MOTT, *Rep. Progr. Phys.* **12** (1948/49) 163.

Received 2 September
and accepted 30 October 1992